# Continuous Beam-Steering Low-Loss Millimeter-Wave Antenna Based on a Piezo-Electrically Actuated Metasurface

Rabbani, Muhammad Saqib; Churm, James; Feresidis, Alexandros P.

*DOI:*
10.1109/TAP.2021.3137248



*Document Version*
Publisher's PDF, also known as Version of record

*Citation for published version (Harvard):*
Rabbani, MS, Churm, J & Feresidis, AP 2022, 'Continuous Beam-Steering Low-Loss Millimeter-Wave Antenna Based on a Piezo-Electrically Actuated Metasurface', *IEEE Transactions on Antennas and Propagation*, vol. 70, no. 4, pp. 2439-2449. https://doi.org/10.1109/TAP.2021.3137248

# Continuous Beam-Steering Low-Loss Millimeter-Wave Antenna Based on a Piezo-Electrically Actuated Metasurface

Muhammad Saqib Rabbani, James Churm, *Member, IEEE*, and Alexandros P. Feresidis, *Senior Member, IEEE*

***Abstract*— A novel antenna beam-steering technology is proposed for emerging millimeter-wave (mm-wave), broadband mobile technologies such as 5G and beyond. A high-gain (23 dBi) antenna with 30° beam steering is designed and tested at around the 38 GHz band. A Fabry–Perot type leaky-wave antenna (LWA) is employed as the main radiating structure, with a tunable high-impedance surface (HIS) used as the ground plane. The HIS phase tuning is accomplished by electro-mechanically varying the displacement between the HIS periodic metasurface layer and the ground plane using a flexure amplified piezoelectric actuator (PEA). The antenna exhibits very low loss (<1 dB) along with fast (in the order of ms.) and continuous beam steering. The measured and simulated results show close agreement and suggest that PEA-tuned, metasurface-based antennas offer a promising solution for use in future mm-wave communication systems.**

***Index Terms*— 5G antenna, antenna beam-steering, Fabry–Perot antenna, high-impedance surface (HIS), leaky-wave antenna (LWA), millimeter-wave (mm-wave) antenna.**

## I. Introduction

MILLIMETER-WAVE (mm-wave) frequencies offer a promising solution for emerging broadband mobile communications such as 5G and beyond. The higher frequencies can accommodate the increasing demand for exceptionally fast data rates (multigigabits/s) over wireless networks [1]. However, as the path losses are high in the mm-wave band, high gain antennas are essential to maintain the link budget [2]. Increasing the antenna gain reduces the spatial coverage of the wireless transmission, which necessitates the antenna to have beam steering properties in order to sustain the wireless link [3].

Based on recent channel measurements at the 5G candidate frequency bands around 28, 38, and 73 GHz, it has been reported that a total antenna gain of about 37 dBi may be required in the link budget, having higher gains (∼25 dBi) at the base station and lower gains (∼12 dBi) at the mobile end [2]. Antenna beam steering of around 45° may be desirable for nonline of sight (NLOS) communication, depending on the number of sectors in a cell of the 5G base station, and up to 10° for a line of sight (LOS) link [1], [2]. An antenna bandwidth of <1 GHz (∼2.63% fractional bandwidth at 38 GHz) may be enough at the base station (along with <5 GHz at 73 GHz band backhaul [4]) to deliver multigigabits per second data rates with conventional modulation techniques. A continuous and fast antenna beam steering as well as low loss performance are required to establish robust 5G mobile communications [5].

The design of high gain beam-steerable antenna exhibiting the aforementioned characteristics at mm-wave frequencies is particularly challenging [6]. State-of-the-art beam steering antenna technologies, i.e., mechanical beam steering, beam switching, electronic beam scanning, etc., are constrained by several factors including upper frequency limit, loss performance, cost, complexity, scanning speed, and resolution [7]–[9]. Conventional phased array techniques employed for beam steering are applicable only at lower mm-wave frequencies due to poor performance and high energy consumption of phase shifters at higher frequencies [8]. Similarly, beam switching/steering methods using p-i-n/varactor diodes are limited to lower mm-wave frequencies and provide a limited number of beams [10], [11]. Tunable materials, such as electro-active polymers [12], ferroelectric [13], and liquid crystals [14]–[16], inherit high losses, slow scanning response, and mechanical stability issues for high resolution and wider scanning angles.

Tunable diode based reconfigurable metasurfaces have also been reported for high gain antenna beam steering using leaky-wave, transmit-array, and reflect-array techniques [17]–[22]. Currently there are several issues to consider with regard to diode technology at mm-wave frequencies, including: availability, the large number of diodes required across the array, high losses, limited scanning range, and severe beam squint. For example, a beam tunable antenna is presented in [17] based on ferroelectric varactor diodes at 12 GHz. The antenna contains 3200 varactor diodes and yields ±10° beam scanning with 4.7 dBi loss. In [18], 4000 varactor diodes are employed to obtain a ±30° beam scanning at the cost of 18 dBi insertion loss at 5 GHz. In tunable metamaterial technology, the antenna beam steering range can be enhanced by stacking the periodic layers, which introduces extra losses to the overall system.

Manuscript received May 8, 2020; revised May 18, 2021; accepted September 23, 2021. Date of publication December 28, 2021; date of current version April 7, 2022. This work was supported by the U.K. Engineering and Physical Sciences Research Council under Grant EP/P008380/1. *(Corresponding author: Muhammad Saqib Rabbani.)*

The authors are with the Metamaterials Engineering Laboratory, School of Engineering, University of Birmingham, Birmingham, B15 2TT, U.K. (e-mail: saqibrabbani05@hotmail.com).

Digital Object Identifier 10.1109/TAP.2021.3137248

Ultimately, this is a tradeoff between the antenna scanning range and losses [17]. In [23], mechanical tuning is employed in reflect-array antenna at 26 GHz to obtain a beam steering of ±60° by tilting the periodic surface from ±30°. The array exhibits several drawbacks including 4 dB losses, 6 dB gain drop, and limited scanning speed. Due to the limitations of current systems, new enabling phase-shifting technologies are in high demand that mitigate these shortcomings, so that robust beam steerable antennas can be designed for mm-wave frequencies.

A tunable, piezoelectric actuator (PEA)-based, high-impedance surface (HIS) was recently developed as an electro-mechanically tuned phase shifter exhibiting relatively low-loss performance in the mm-wave band [24], [25]. However, the reported HIS square ring unit cell geometry in [21], [24], and [25], utilized a small amount of displacement (18 $\mu$m) and exhibited very narrowband (<1% bandwidth for over 100° phase shift) operation. In addition, a similar narrowband tunable HIS was used, in simulations only, for a beam steered antenna application [25]. This was a very narrowband leaky-wave antenna (LWA) structure, resulting in a medium directivity (16.4 dBi), and using an impractical ideal dipole feeding element, where impedance matching, losses, and total antenna gain are not discussed. The narrowband nature of the HIS in that LWA antenna caused severe beam squint (>15°/100 MHz), which is not desirable for most applications. More recently, a brief design concept and some initial simulation results were presented on more broadband tunable HIS and LWAs based on improved designs [26]–[28].

In this article, a low loss (<1 dB) and broadband electromechanically tuned phase-shifting HIS is presented and employed within a Fabry–Perot type LWA for continuous beam steering of 33° with a high gain of 24 dBi at around 38 GHz. The desired phase shifting is accomplished by varying the gap between a HIS periodic layer and a ground plane. A flexure amplified PEA is used to tune an optimized HIS that produces over 150° reflection phase shift, over a very wide bandwidth. This is a crucial development over previous narrowband PEA based tunable HIS designs, which, if incorporated into a LWA, would limit the antenna bandwidth and cause wide angle beam squint. The development of a wideband HIS enables a LWA antenna to be designed with exceptionally low loss performance (<1 dB) and wide beam steering range across a broad bandwidth (1 GHz). A balun-fed printed dipole antenna is employed as the feeding element of the LWA, and an acceptable impedance matching is achieved over the operating band.

A detailed discussion is presented on the theoretical development of the proposed HIS design, partially reflective surface (PRS), and overall LWA structure. A complete mechanical integration of the tunable HIS, PRS, dipole feed, and PEA is also presented, along with comprehensive measurements and characterization of the HIS, balun dipole, and overall LWA across the 5G candidate frequency band around 38 GHz. The simulated and measured results show good agreement in all cases, and suggest that PEA enabled metamaterial based antennas are a promising solution for future mm-wave communication systems.

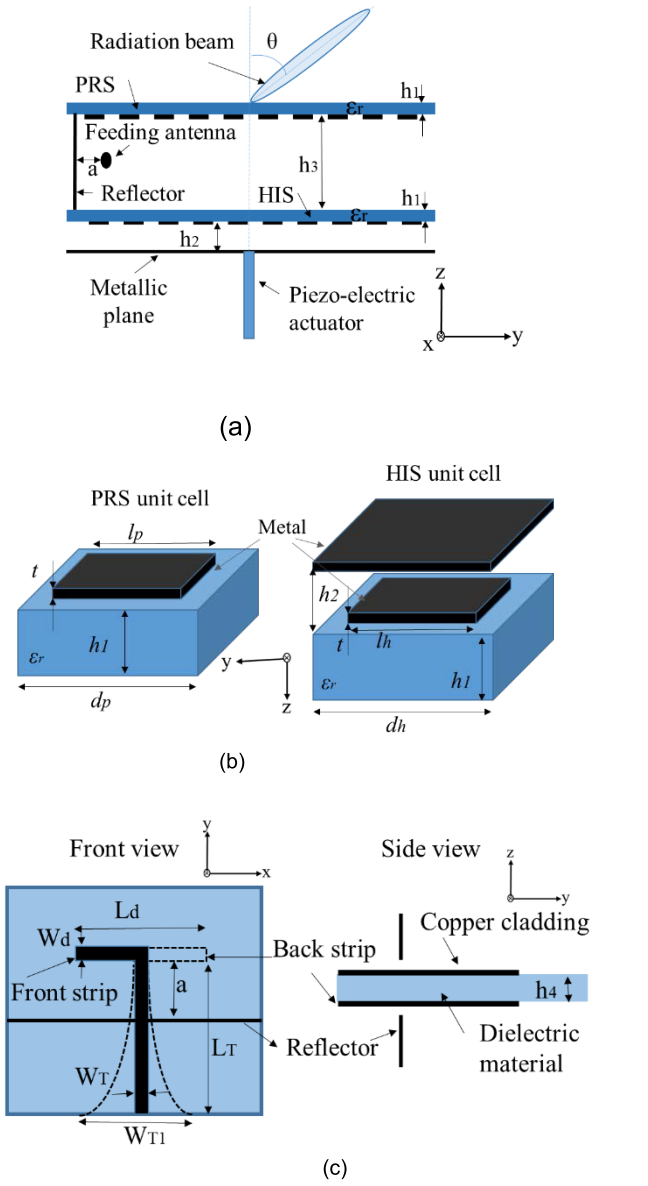


Fig. 1. Geometry of the proposed LWA. (a) Overall antenna schematic, (b) PRS and HIS unit cells, and (c) feeding dipole element (Dimensions not to scale).

This article is organized as follows: Section II describes the antenna design procedure, Section III deals with the HIS phase shifter measurements, Section IV demonstrates the antenna measurement results, and finally, Section V concludes the work.

## II. Antenna Design

Fig. 1 illustrates the geometry of the proposed LWA design where Fig. 1(a)–(c) presents the overall antenna schematic, PRS and HIS unit cells, and the feeding dipole element, respectively. The antenna comprises a HIS-enhanced Fabry–Perot-type leaky wave cavity, which is formed by the gap between a PRS (top) and a HIS (bottom). The leaky-wave cavity is excited through a printed circuit dipole element, placed on one side of the cavity and backed by a metallic reflector. The HIS metasurface comprises a sheet of periodic

metallic square patches, suspended over a metal ground plane at distance $h_2$. The periodic layer of the HIS is mechanically fixed to the rest of the antenna structure and is placed in close proximity to the metallic plane, which is mounted on a PEA so that the distance $h_2$ can be varied when a voltage is applied. The change in relative displacement between the HIS periodic layer and the ground plane causes the phase response of the HIS to shift, which is used to control the beam angle as explained in detail in this section. The theoretical aspects of the beam scanning property of a LWA are expressed in [29] in detail.

### *A. Feed Antenna*

The feeding antenna is a half-wavelength dipole element printed on a low-loss substrate (RT/Duroid 5880) with $\varepsilon_r = 2.2$, thickness $h_4 = 0.127$ mm and copper cladding thickness of 17.5 $\mu$m, as shown in Fig. 1(c). Half of the dipole length was etched on the top of the substrate and the other half was etched on the bottom. The antenna was connected to a standard 50 $\Omega$ input through a balun microstrip line with a tapered ground, as described in [30]. The feeding antenna dimensions are as follows: $L_d = 3$ mm, $W_d = 0.5$ mm, $L_T = 4$ mm, $W_T = 0.3$ mm, $W_{T1} = 0.5$ mm, with a PCB area of 6 mm $\times$ 6 mm. Fig. 2(a)–(c) present the simulated $S_{11}$, far-field radiation patterns (FRPs) at 38 GHz in E- and H-planes, and in three-dimensions. As seen from Fig. 2, the dipole antenna $-10$ dB $S_{11}$ bandwidth, directivity, and efficiency are about 6 GHz (i.e., 15% fractional bandwidth), 7.44 dBi, and 95%, respectively. The bandwidth spans between 36 and 42 GHz, which is well above the desired 1-GHz bandwidth for 5G applications. Moreover, it is expected that the feeding antenna directivity may be further enhanced due to the placement of a larger reflector, when implemented in the final LWA structure.

### *B. PRS and HIS*

The PRS and HIS consist of metallic square patch elements, etched onto the same substrate material as the feed antenna (RT/Duroid 5880), but with substrate thickness, $h_1$, of 0.787 mm and copper cladding of 35 $\mu$m. The PRS is designed to exhibit a high-reflection coefficient magnitude ($\Gamma = 0.93$) in order to obtain high antenna directivity with a reasonable fractional bandwidth ($BW = 2.7\%$, corresponding to 1 GHz bandwidth around 37 GHz central frequency) according to the expressions given in [31] and [32]. It should be noted that this analysis assumes infinite size surfaces. The optimized PRS unit cell dimensions are $l_p = 3$ mm and $d_p = 3.3$ mm [see Fig. 1(b)]. Fig. 3 shows the simulated magnitude and phase response of the infinite periodic PRS reflection coefficients under normal plane wave incidence, where it can be seen that $\Gamma$ remains around 0.935% for frequencies between 36 and 38 GHz. It is therefore predicted that the proposed PRS will boost the feeding antenna directivity (7.4 dBi) by 15 dB, increasing the maximum LWA directivity to 22.5 dBi. It has been found that this predicted directivity is approximately achievable in practice with large enough array sizes for the PRS, ($>20 \times \lambda$) [33], [34]. The resonant cavity height, $h_3$, was initially set to be half of the operating wavelength ($\lambda/2 = 3.95$ mm) and then it was optimized to be 3.5 mm in CST Microwave Studio for maximum directivity and resonance at 38 GHz.

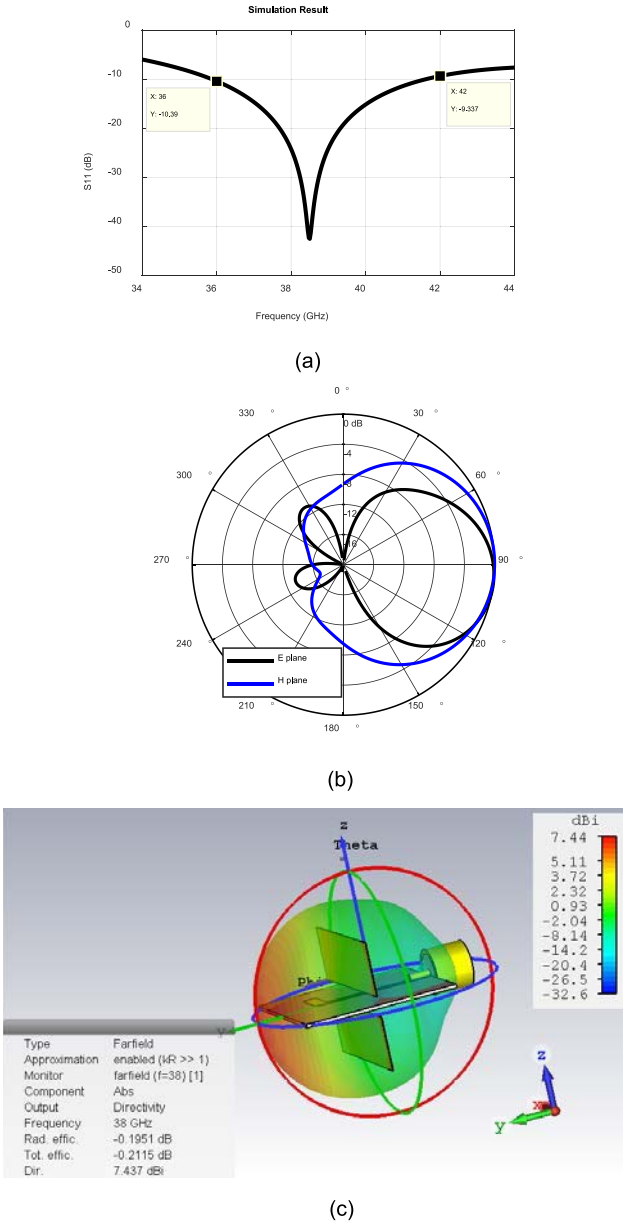


Fig. 2. Feeding dipole antenna simulation results. (a) $S_{11}$, (b) E- and H-plane radiation patterns at 38 GHz, and (c) 3-D radiation pattern at 38 GHz.

The HIS is designed to achieve a broadband highly tunable reflection phase ($\varphi_{HIS}$) response, sensitive to the separation between HIS periodic layer and ground plane, $h_2$. The HIS reflection coefficient phase can be approximated by

$$\varphi_{HIS} = 2\varphi_T - \frac{4\pi}{\lambda} \cdot h_2 - \pi \tag{1}$$

where $\varphi_T$ is the phase of transmission coefficient of HIS periodic layer and $\lambda$ is the operating wavelength [24]. Thus, $\varphi_{HIS}$ is a function of $\varphi_T$, which depends on the geometry of the periodic unit cell. A detailed theoretical analysis and

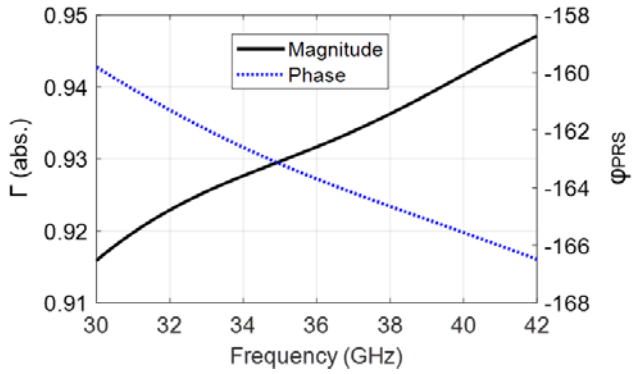


Fig. 3. Magnitude and phase response of PRS reflection coefficients.

designing process of a static square patch-based HIS is presented in [35] and [36] and bandwidth and loss performance has been analyzed for various unit cell dimensions. Using the similar designing approach, the HIS unit cell dimensions are initially set to be an adequate fraction of the operating frequency i.e., $l_h \approx \lambda/5, h_2 \approx \lambda/10$ and $d_h \approx l_h + l_h/5$, and the optimal $\varphi_T$ was achieved with dimensions of $l_h = 1.53$ mm and $d_h = 1.83$ mm. Here, an important modification is made in the proposed HIS unit cell, as compared to the ones in [35] and [36] that the dielectric layer is moved to the opposite side of the periodic layer and a widely tunable air gap, $h_2$, is introduced between the periodic and metallic layers to tune the HIS phase response. An amplified piezo-actuator is employed to adjust the air gap, $h_2$, of the optimal HIS while maintaining its wideband operation. The separation, $h_2$, is varied from 40 to 400 $\mu$m to achieve the desired HIS-reflected phase shift, $\varphi_{HIS}$. Fig. 4(a) and (b) depicts the simulated magnitude and unwrapped phase response of the HIS reflection coefficients, respectively. Fig. 4 shows that the change in separation from 0 to 40 $\mu$m does not make a significant difference in the HIS reflection magnitude (return loss) response. However, separations between 40 and 400 $\mu$m ($\Delta h_2 = 360$ $\mu$m) yield a phase shift of about $\Delta\varphi_{HIS} = 156°$ at 38 GHz whilst exhibiting negligible loss of about 0.03 dB. The HIS produces relatively smaller phase shift at the lower frequencies as compared to higher frequencies (e.g., $\Delta\varphi_{HIS} = 142°$ at 37 GHz and $\Delta\varphi_{HIS} = 132°$ at 36 GHz).

### C. Antenna Operation

The resonance condition of the proposed LWA was obtained by setting the Fabry–Cavity height, $h_3$, equal to approximately half of the operating wavelength. The power radiation pattern can be initially calculated approximately through a ray-optic technique assuming infinite size of the antenna [25], [37]

$$P = \frac{1-\Gamma^2}{1+\Gamma^2-2\Gamma\cos\left(\varphi_{PRS}-\varphi_{HIS}-\frac{4\pi}{\lambda}\cdot h_3\cdot\cos(\theta)\right)}\cdot F(\theta)^2 \quad (2)$$

where $F(\theta)$ is the radiation pattern of the feeding element, $\Gamma$ and $\varphi_{PRS}$ are the magnitude and phase of the reflection coefficients of PRS, respectively. A detailed theoretical analysis including dispersion diagrams of this type of LWA has been

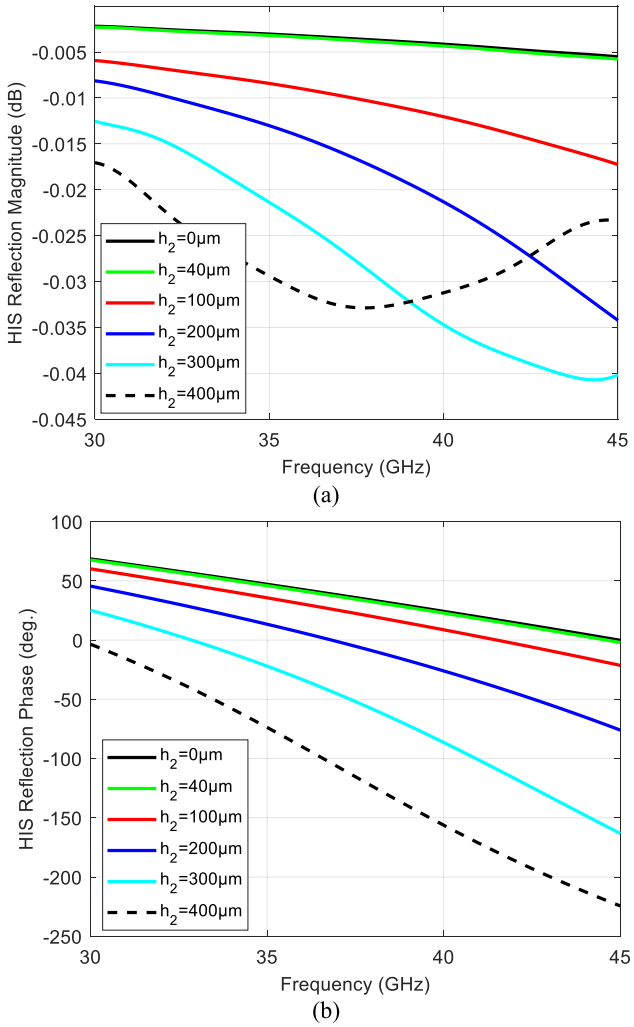


Fig. 4. Simulation results of (a) magnitude and (b) phase response of HIS reflection coefficients.

presented in [38] and [39]. It is clear from (2) that the proposed LWA radiation performance is determined by the PRS, HIS, and separation between the two. The FRP of a half-wavelength dipole antenna at boresight angle ($\theta_d$) having metallic reflector at distance, $a$, is approximated as

$$F(\theta) = \cos\left(\theta_d + \frac{\pi}{2}\right)\cdot\cos\left[\frac{\beta}{2}\cdot a\cdot\cos\left(\theta_d+\frac{\pi}{2}+\pi\right)\right] \quad (3)$$

where $\beta = 2\pi/\lambda$ is the wavenumber [25]. The FRP and beam scanning range of the proposed LWA is predicted at 36, 37, and 38 GHz by substituting the corresponding values of $\Gamma$, $\varphi_{PRS}$ and $\Delta\varphi_{HIS}$ from Figs. 3 and 4(b). Table I summarizes the predicted beam-steering performance of the LWA at the mentioned frequencies where it can be seen that antenna may exhibit a beam steering of about 34° at 38 GHz. It can also be noticed that the beam scanning range is a few degrees larger at the lower frequencies (e.g., 38° at 37 GHz and 39° at 36 GHz).

Using the proposed geometry, the LWA was modeled and simulated in CST Microwave Studio. The PRS and HIS layers comprised of 9 × 27 and 16 × 49 unit cells, respectively, (approximately a 3 cm × 9 cm area, which is significantly greater than the wavelength, $\lambda = 0.8$ cm). Fig. 5(a) and (b)

TABLE I
LWA BEAM SCANNING PREDICTION

| Frequency (GHz) | $\Delta\varphi_{HIS}$ (°) | Beam scanning (°) | Beam scanning range (°) |
|---|---|---|---|
| 36 | 132 | 39° | 9°-49° |
| 37 | 142 | 38° | 14°-52° |
| 38 | 156 | 34° | 22°-58° |

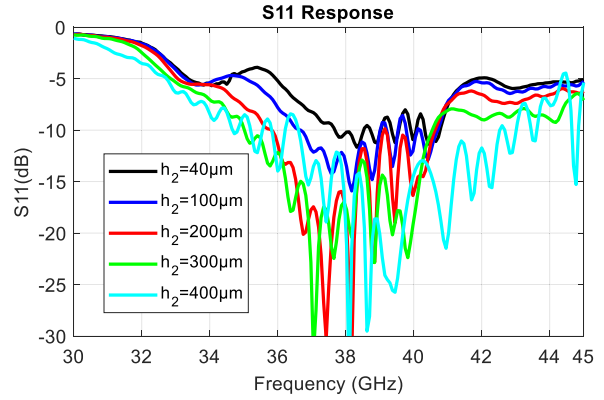


(a)

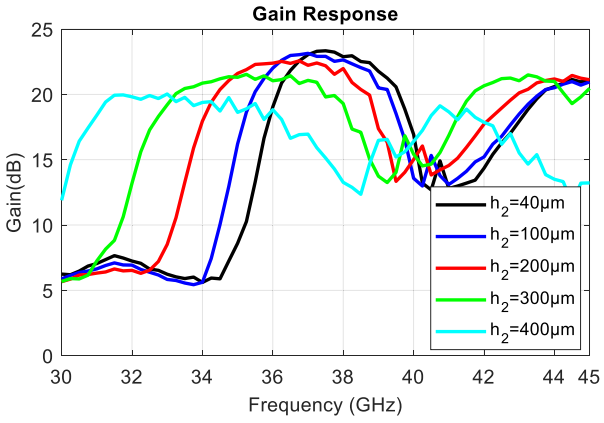


(b)

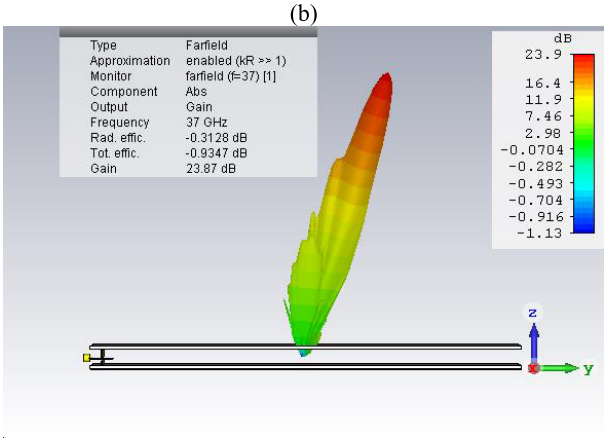


(c)

Fig. 5. LWA simulation results. (a) $S_{11}$, (b) gain response for various displacements, and (c) 3-D FRP at 37 GHz with $h_2 = 40$ $\mu$m.

shows the simulated antenna $S_{11}$ and gain response, for separation, $h_2$, from 40 to 400 $\mu$m. Fig. 5(c) presents the 3-D FRP at 37 GHz with $h_2 = 40$ $\mu$m. It can be seen in Fig. 5(a) that the $S_{11}$ magnitude remains below $-10$ dB over the range of displacements across a 1 GHz bandwidth between 37 and 38 GHz. The antenna gain stays above 19.5 dBi with a 1-GHz operating bandwidth up to a separation of 300 $\mu$m; it then drops sharply due to a shift in gain at lower frequencies. The maximum gain at 37 GHz is 23.78 dBi (24.7 dB directivity) for $h_2 = 40$ $\mu$m. The LWA simulated directivity is about 2 dB higher than the predicted one, in Section II-B, which is likely due to the directivity enhancement of the feeding element because of the larger reflector used in the full LWA simulation and the presence of the HIS and PRS in the surroundings. The antenna simulation total efficiency remains above 80% from 36 to 38 GHz for most of the displacements. Fig. 6(a)–(c) demonstrate the normalized simulated H-plane FRP and beam steering performance of the LWA at 36, 37, and 38 GHz, showing highly directive FRP with scanning ranges of 30° and 28° at 37 and 38 GHz. The maximum beam scanning response of 33° (i.e., from 10° to 43°) is at 36 GHz and for all angles is within 3 dB loss with respect to the peak gain. It can be noticed that the beam scanning range of the simulated LWA in Fig. 6 is fairly close to the one predicted in Table I, with similar scanning trend across the mentioned frequencies. The sidelobe level (SLL) is below $-10$ dB for lower displacements and rises to –6 dB for the largest separation (400 $\mu$m) at 36 GHz. The FRP becomes distorted at 38 GHz due to the shift in peak gain to lower frequencies. The LWA exhibits a beam squint of between 3° and 6° within a 1-GHz operating bandwidth, having larger beam squint at lower separation. It is found from the simulated results that the beam squint improves down to only 2° when the operating bandwidth is reduced to 500 MHz around 37 GHz, making this the best operational band for the proposed antenna. Fig. 6(d) presents the normalized E-plane FRP simulated results of the LWA at 37 GHz, and shows that the FRP in E-plane remains at broadside across the operating frequency band.

## III. HIS PHASE SHIFTER MEASUREMENTS

To test the configurability of the HIS in isolation from the rest of the LWA, and to demonstrate the feasibility of a PEA tuned device, the HIS was patterned onto a RT/Duroid5880 substrate with 35 $\mu$m rolled copper cladding. Unit cell dimensions were as described in Section II. The unit cell was repeated in an array of 91 $\times$ 91 units, approximately an overall size of 20 $\times$ 20 wavelengths at 37 GHz, to produce a surface measuring 16.6 $\times$ 16.6 cm. The measured HIS is significantly larger than that in the final LWA for ease of measurement. The full HIS, which was fabricated in-house using standard PCB techniques, can be seen in Fig. 7(a). Due to its size, the substrate was not mechanically strong enough to be suspended over the ground plane without significant sagging. To combat this, the back side of the substrate was bonded, with a small amount of epoxy, to a piece of 20 mm thick Rohacell foam, with a dielectric constant of 1.08 at 26.5 GHz, and a loss tangent of 0.004. This improved the mechanical stability of the HIS without adversely affecting the dielectric properties of the substrate.

The HIS is tuned by varying the separation between the periodic surface and ground plane, $h_2$ in Fig. 1(b). This is

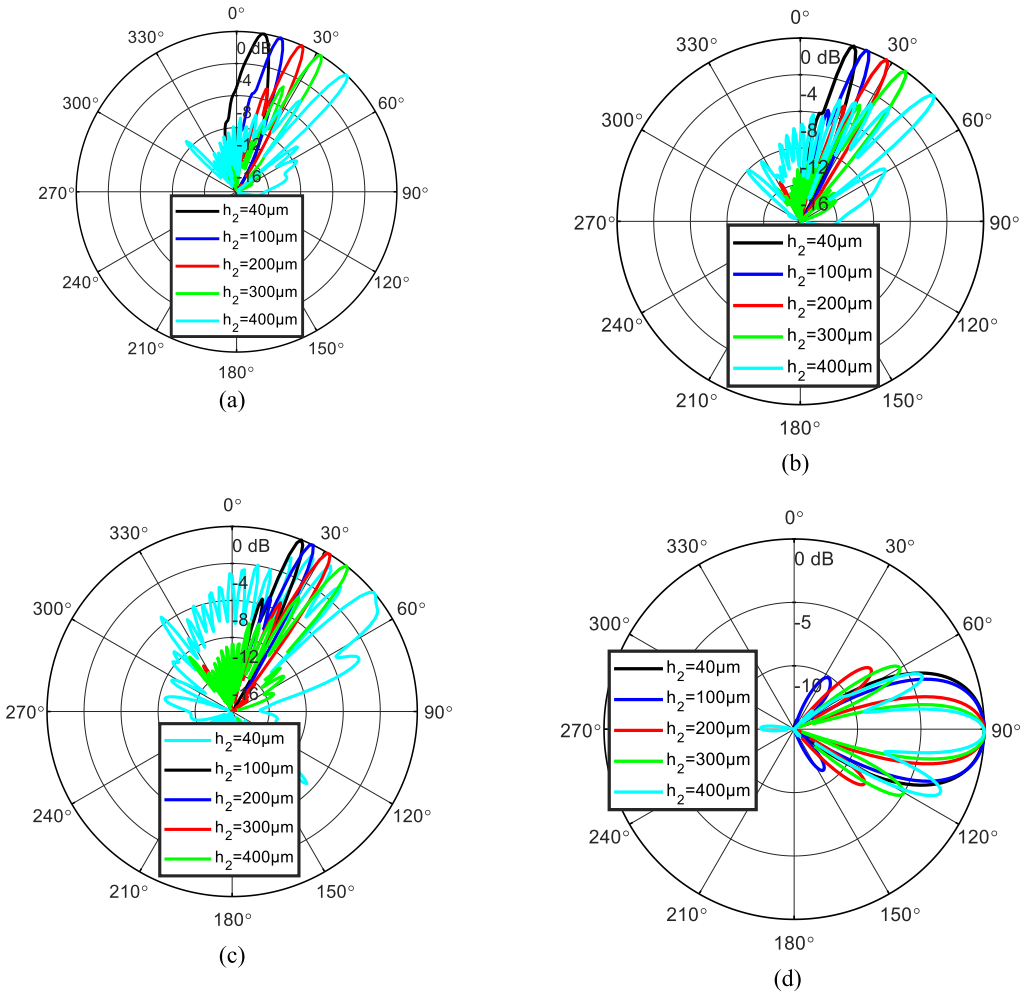


Fig. 6. Normalized LWA FRP simulation results and beam-steering performance. With H-plane at (a) 36 GHz, (b) 37 GHz, and (c) 38 GHz, and E-plane FRP at (d) 37 GHz.

enabled by a flexure amplified PEA (PiezoMove P-603, Physik Instrumente Ltd., U.K.), which can provide displacement of up to 500 $\mu$m and can be seen in Fig. 7(b). By applying a voltage of up to 120 V, the PEA can provide millisecond switching and nanometer accurate displacement. The PEA was mounted on a fixed metal stand and attached to a 3-mm thick aluminum sheet measuring 125 mm $\times$ 125 mm, which was used as the metallic ground plane of the HIS. The periodic surface was suspended over this metallic plane where the initial separation could be controlled. The PEA was fully energized by the application of 120 V, supplied by a standard variable power supply. The ground plane was then elevated so that it touched the bottom of the periodic layer, ensuring that the relative alignment between the two was maintained. The voltage applied to the PEA was then reduced to 0 V to provide a 500 $\mu$m gap between the two surfaces.

Before measurements were performed, the periodic surface was removed from the system so that normalization measurements could be taken using the bare ground plane for each of the desired voltages. The periodic surface was then carefully returned and each measurement could be taken with respect to the corresponding bare ground measurement for the correct separation.

Two horn antennas were setup, as shown in Fig. 7(c) and (d), so that the periodic surface was in the far-field. The angle of incidence of each horn antenna was set to be less than 10° from normal. Using a vector network analyzer (ZVA67, Rohde and Schwarz) the transmitting horn antenna was swept between 36 and 38 GHz with the receive channel setup to log reflected phase and magnitude. The $S_{21}$ magnitude and phase response was measured while varying the voltage applied to the PEA between 120 and 0 V, which altered the separation between ground plane and HIS periodic layer between 0 and 460 $\mu$m.

Both magnitude and phase of the reflection measurement can be seen in Fig. 8(a) and (b). Fig. 8(a) shows that the measured HIS losses vary between 1 and 0.21 dB depending on displacement. This is slightly higher than simulated losses due to the additional Rohacell, which was confirmed by subsequent resimulation of the unit cell.

A maximum phase shift of 151° is observed around 38 GHz over the full displacement. If compared directly to expectations, the phase shift for the displacement between 45 and 400 $\mu$m at 37 GHz is 115°, which is 27° lower than in simulation. This discrepancy is mainly due to small misalignments between the HIS array and the ground plane. Other

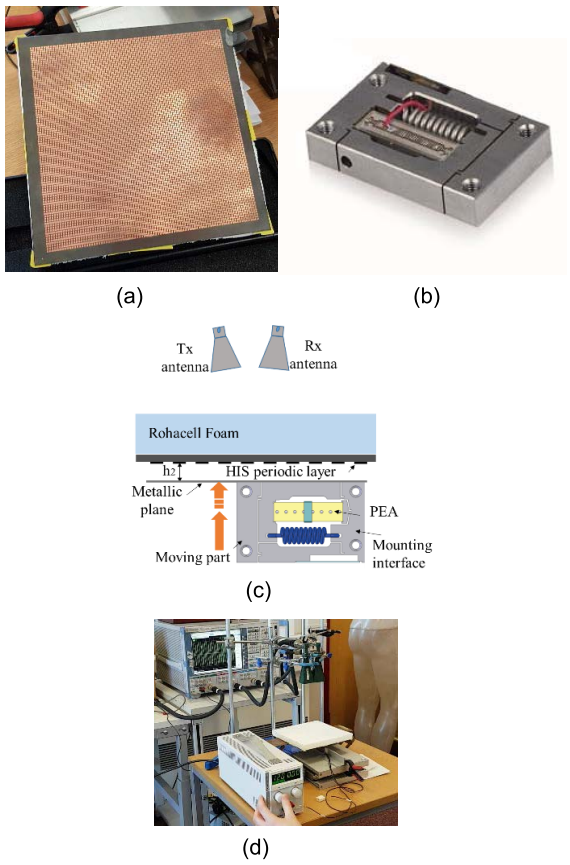


Fig. 7. HIS measurements using PEA. (a) Fabricated HIS periodic layer, (b) photograph of the employed PEA, (c) schematic of the HIS and PEA implementation (not in scale), and (d) experimental setup.

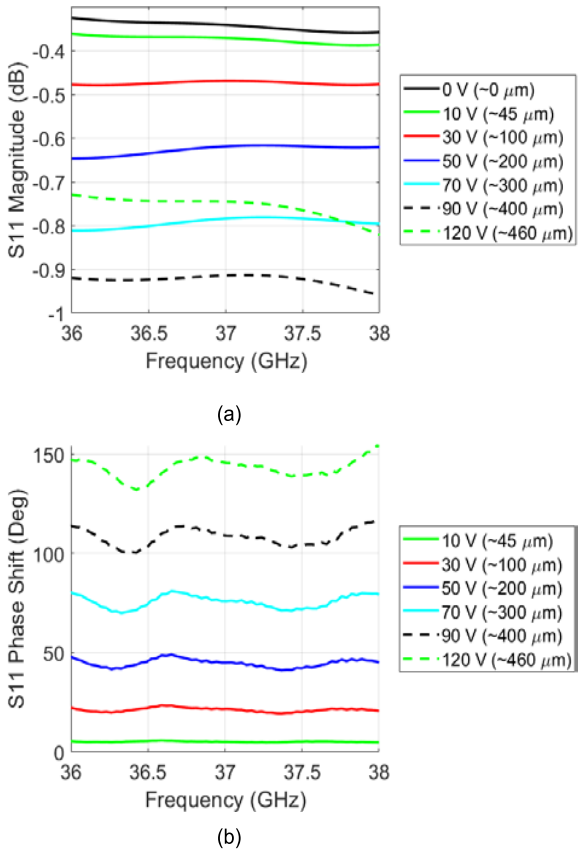


Fig. 8. Measured results of the HIS reflection coefficients. (a) Reflected magnitude and (b) phase shift response relative to the 0 V measurement.

factors include slight inaccuracies with the in-house PCB etching process and tolerances of the experiment fixtures. Rohacell was not used in the final LWA assembly, therefore the additional losses will not be present. Along with this, alignment will be easier in the final structure due to the smaller size of the HIS. It was therefore expected that the HIS performance would improve *in situ*, and the measured LWA's beam scanning range would not be significantly affected.

The proposed reconfigurable HIS is one of the lowest loss tunable phase-shifting artificial surfaces presented in the literature at these frequencies. It is expected that the phase-shifting performance of this surface can be improved further by designing more displacement sensitive periodic geometries and by employing more sophisticated fabrication processes. It is also possible to scale such a quasi-optical phase shifter to much higher mm-wave frequencies and beyond, into the terahertz band.

## IV. Antenna Measurements and Discussions

Fig. 9(a)–(c) demonstrates the fabricated feeding antenna, experimental setup for $S_{11}$ measurement, and the simulated and measured $S_{11}$ response of the printed dipole feeding antenna. As seen from Fig. 9(b), the antenna is connected to the ZVA67 VNA through a 1.85-mm flange launcher and its associated Glass Bead (GB185). The Glass Bead reduces the interaction of the connector's body to the small radiation element by introducing an extra separation between them. From Fig. 9(c) it is clear that the measured and simulation $S_{11}$ responses show a similar trend, offering a wide bandwidth around the resonant frequency of 38 GHz. It can be noticed that the dipole-measured bandwidth is wider than the simulated antenna. This discrepancy in the simulation and measured results is attributed to low-cost PCB-etching fabrication tolerances for the fine antenna PCB details and the presence of connector body close to the radiating element. Nevertheless, the $S_{11}$ remains below $-10$ dB across the LWA's target operating bandwidth from 36 to 38 GHz.

Based on the presented PRS, HIS, and feeding antenna structures shown in Section II, the final LWA design was prepared and tested. A Nylon frame was designed to hold the PRS and HIS layers, as well as to accommodate the feeding antenna and its associated connector components. Fig. 10(a) and (b) shows the final LWA assembled with the PEA and the antenna prototype during FRP measurements, respectively. For antenna beam-steering measurements, the PEA-biasing voltage was tuned from 0 to 120 V with a step of 20 V. The corresponding displacement for each voltage step was not determined at this stage.

Fig. 11(a) reveals the measured $S_{11}$ responses of the LWA for various voltages. It shows that the antenna's $S_{11}$ remains consistently below $-10$ dB from 34 to 38.5 GHz for all displacements. However, comparing Figs. 5(a) and 11(a), it can be

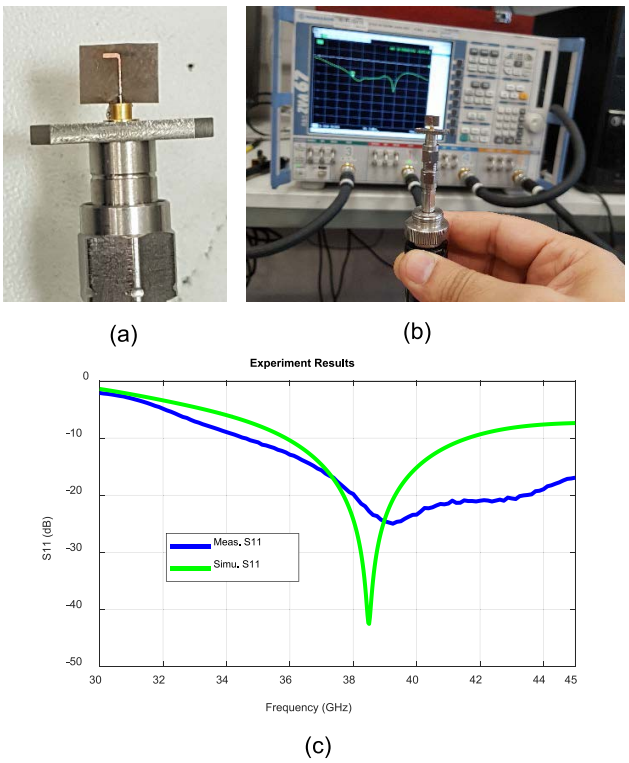


Fig. 9. Feeding printed dipole antenna measurement. (a) Fabricated prototype, (b) experimental setup, and (c) simulated and measured $S_{11}$ results.

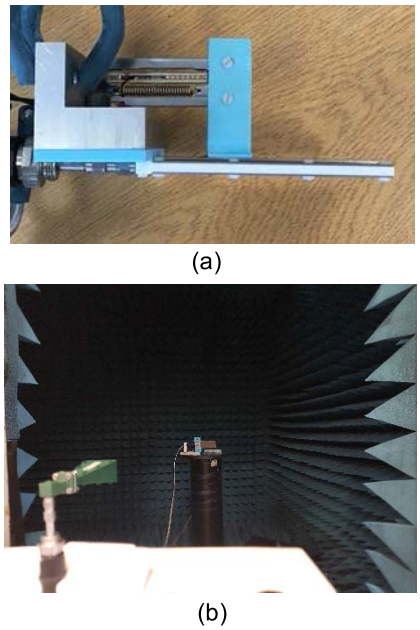


Fig. 10. Beam-steerable LWA assembly for measurements. (a) Shows the fabricated prototype and (b) shows the experimental setup for FRP measurements, respectively.

noticed that there is about a 2 GHz shift in the overall resonant frequency band, which may be due to inconsistencies and misalignments in the resonant cavity height, $h_3$, due to uneven PRS and HIS layers, as at the antenna center there is less mechanical support for the layers. Fig. 11(b)–(d) demonstrates the measured FRPs of the LWA in H-plane at the representative

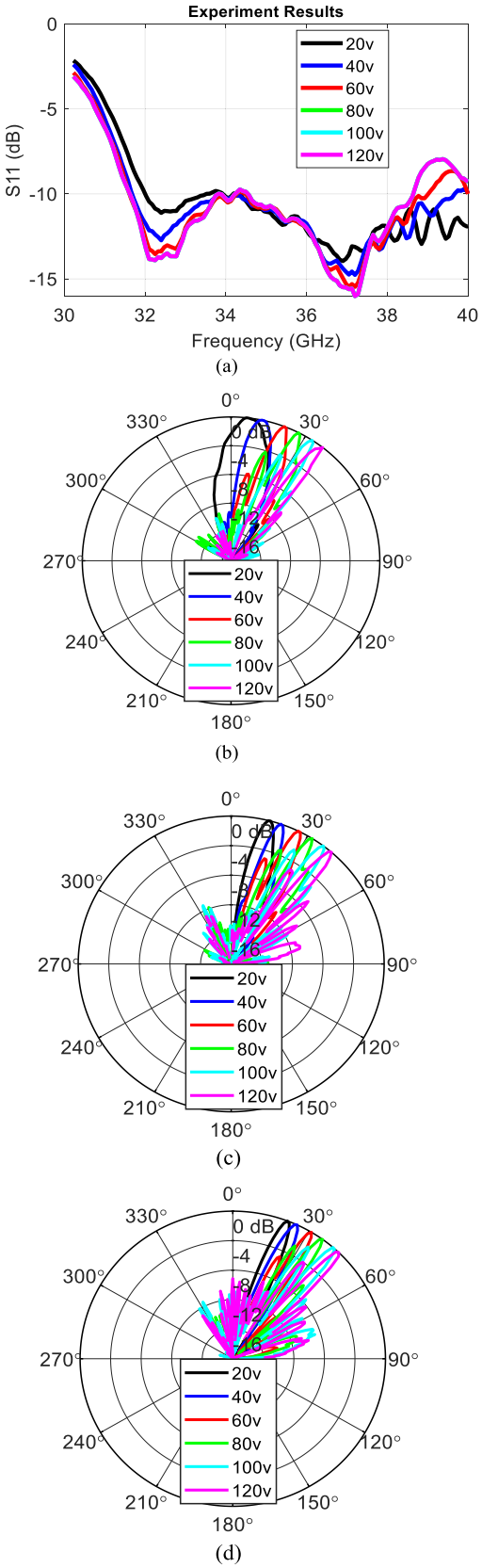


Fig. 11. Beam steerable LWA results. (a) $S_{11}$, and beam scanning in H-plane at (b) 34 GHz, (c) 35 GHz and (d) 36 GHz with various displacement.

measured frequencies, i.e., 34, 35, and 36 GHz, respectively, for the different displacements. The antenna depicts highly directive FRPs, as expected, with a scanning range of 32°, 27°,

TABLE II
LWA-MEASURED FRP PERFORMANCE

| LWA results | Max. Gain (dBi) | Min. HPBW (°) | Beam scan. (°) | Scan. range (°) | Beam squint (°) | BW (GHz) |
|---|---|---|---|---|---|---|
| Simu. | 23.78 | 3-5 | 30 | 17-47 | 6 | 1 |
| Meas. | 23.11 | 3-5 | 27 | 14-41 | 7 | 1 |

TABLE III
COMPARISON OF THE REPORTED AND PROPOSED BEAM-STEERING ANTENNAS. (ABBREVIATIONS: DIELECTRIC ELASTOMER ACTUATOR (DEA), REFLECT-ARRAY (R-A), TRANSMIT-ARRAY (T-A), VARACTOR DIODE (VD), FERROELECTRIC (FE), LIQUID CRYSTAL (LC), SUBSTRATE INTEGRATED WAVEGUIDE ARRAY (SIW-A)

| Ref. | [12] | [13] | [22] | [41] | [42] | Prop. |
|---|---|---|---|---|---|---|
| Antenna type | R- A | LWA | T- A | SIW- A. | R- A | LWA |
| Tuning technique | DEA | FE | VD | VD | LC | PEA |
| Operating frequency (GHz) | 30 | 92 | 22 | 6 | 78 | 38 |
| Gain (dBi) | <20 | 6 | 3 | 10 | 25 | 23 |
| Beam steering range (°) | 10 | 7 | ±10 | ±45 | ±6 | 30 |
| Phase shifter insertion loss (dB) | >2.6 | <6 | 4.7 | 3.5 | 18 | <1 |

and 23° at 34, 35, and 36 GHz, respectively. The SLL remains below −16 dB for the smaller separations at lower frequencies, and becomes more severe for the larger separations at the higher frequencies, as expected (see Fig. 6).

By comparing Figs. 5 and 6, and 11, it can be seen that both the simulated and measured FRP results show a similar trend in the antenna $S_{11}$ and beam scanning. Table II summarizes the measured FRP performance at 35 GHz and simulation FRP at 37 GHz (a 2 GHz shift in measured frequency band is applied). It is obvious from Table II that the measured results are in close agreement with simulations, except that there is an overall 10° up shift in FRP response of the measured LWA which is likely due to fabrication tolerances. To the best of the author's knowledge, the high gain beam steerable LWA exhibits the best set of performance features, so far presented, at mm-wave frequencies in terms of low loss and low beam squint [40]. Table III compares the proposed antenna performance with the reported beam steering antenna based on other state-of-the-art tuning techniques. It is clear from Table II that the presented electro-mechanically tuned HIS-based beam steering antenna exhibit the lowest loss performance offering a continuous beam steering to a wide angular range. The LWA shown here is a good candidate for fulfilling the key requirements for emerging broadband mobile communication systems at mm-wave frequencies, as outlined in Section I.

## V. CONCLUSION

A high gain LWA is presented at mm-wave frequencies with continuous and fast beam steerable (∼30°) capabilities, providing low-beam squint (6°) across 1 GHz of operating bandwidth and very low-loss (<1 dB) performance for 5G applications. To the authors' knowledge, this is the lowest loss ever reported for beam-steered antennas at these frequency bands. The antenna is designed based on a tunable HIS and fed through a compact printed dipole antenna. A theoretical analysis is performed to predict the proposed LWA performance. The tuning of the HIS is carried out utilizing a PEA by varying an applied voltage. The tunable HIS and feed antenna are first tested individually and then the final LWA prototype is fabricated and tested at the 38-GHz band. The simulation and measured results showed good agreement. Since the beam scanning becomes more sensitive to the displacement between the HIS periodic layer and the metallic plane at higher frequencies, the proposed concept is particularly useful for low-loss beam steerable antenna designs at higher mm-wave and terahertz frequencies. In future research the antenna may be designed at higher frequency bands with an even wider scanning range, enabled by PEA based tuning.

## ACKNOWLEDGMENT

The authors would like to thank A. Yates and J. Sangha for their support in prototype fabrication.

## REFERENCES

[1] A. I. Sulyman, A. T. Nassar, M. K. Samimi, G. R. MacCartney, Jr., T. S. Rappaport, and A. Alsanie, "Radio propagation path loss models for 5G cellular networks in the 28 GHz and 38 GHz millimeter-wave bands," *IEEE Commun. Mag.*, vol. 52, no. 9, pp. 78–86, Sep. 2014.

[2] T. S. Rappaport *et al.*, "Millimeter wave mobile communications for 5G cellular: It will work!" *IEEE Access*, vol. 1, pp. 335–349, 2013.

[3] W. Roh *et al.*, "Millimeter-wave beamforming as an enabling technology for 5G cellular communications: Theoretical feasibility and prototype results," *IEEE Commun. Mag.*, vol. 52, no. 2, pp. 106–113, Feb. 2014.

[4] M. Shafi *et al.*, "5G: A tutorial overview of standards, trials, challenges, deployment, and practice," *IEEE J. Sel. Areas Commun.*, vol. 35, no. 6, pp. 1201–1221, Jun. 2017.

[5] M. K. Samimi, S. Sun, and T. S. Rappaport, "MIMO channel modeling and capacity analysis for 5G millimeter-wave wireless systems," in *Proc. 10th Eur. Conf. Antennas Propag. (EuCAP)*, Davos, Switzerland, Apr. 2016, pp. 1–5.

[6] M. E. Shorbagy, R. M. Shubair, M. I. Al Hajri, and N. K. Mallat, "On the design of millimetre-wave antennas for 5G," in *Proc. 16th Medit. Microw. Symp. (MMS)*, Abu Dhabi, United Arab Emirates, Nov. 2016, pp. 1–4.

[7] C.-C. Sun and H.-T. Chou, "Summary and progress of mm-wave antenna technologies for 5G application," in *Proc. IEEE Int. Symp. Radio-Freq. Integr. Technol. (RFIT)*, Taipei, Taiwan, Aug. 2016, pp. 1–3.

[8] M. Cai, C. He, X. Li, and G. Yang, "Design of mm-wave phased array in mobile terminal for 5G mobile system," in *Proc. Prog. Electromagn. Res. Symp. (PIERS)*, Shanghai, China, Aug. 2016, pp. 2456–2458.

[9] I. Uchendu and J. R. Kelly, "Survey of beam steering techniques available for millimeter wave applications," *Prog. Electromagn. Res. B*, vol. 68, pp. 35–54, 2016.

[10] M. Bouslama, M. Traii, T. A. Denidni, and A. Gharsallah, "Beam-switching antenna with a new reconfigurable frequency selective surface," *IEEE Antennas Wireless Propag. Lett.*, vol. 15, pp. 1159–1162, 2016.

[11] L. Dussopt, "Transmitarray antennas," in *Aperture Antennas for Millimeter and Sub-Millimeter Wave Applications*. Cham, Switzerland: Springer, 2018, pp. 191–220.
[12] P. Romano, "Adaptive millimeter-wave and THz antenna devices based on dielectric elastomer actuators," M.S. thesis, EPFL, Lausanne, Switzerland, 2015, no. 6743.
[13] D. Nyzovets and Y. Yashchyshyn, "A mm-wave beam-steerable leaky-wave antenna with ferroelectric substructure," in *Proc. 13th Eur. Conf. Antennas Propag. (EuCAP)*, Krakow, Poland, 2019, pp. 1–3.
[14] W. Fuscaldo, S. Tofani, P. Burghignoli, P. Baccarelli, and A. Galli, "Terahertz leaky-wave antennas based on metasurfaces and tunable materials," in *Metamaterials Metasurfaces*. London, U.K.: IntechOpen, 2018, pp. 93–116.
[15] B. Sanadgol, S. Holzwarth, and J. Kassner, "30 GHz liquid crystal phased array," in *Proc. Loughborough Antennas Propag. Conf.*, Loughborough, U.K., Nov. 2009, pp. 589–592.
[16] S. Foo, "Liquid-crystal-tunable metasurface antennas," in *Proc. 11th Eur. Conf. Antennas Propag. (EUCAP)*, Paris, France, Mar. 2017, pp. 3026–3030.
[17] T. Jiang, Z. Wang, D. Li, J. Pan, B. Zhang, J. Huangfu, Y. Salamin, C. Li, and L. Ran, "Low-DC voltage-controlled steering-antenna radome utilizing tunable active metamaterial," *IEEE Trans. Microw. Theory Techn.*, vol. 60, no. 1, pp. 170–178, Jan. 2012.
[18] R. Guzman-Quiros, J. L. Gomez-Tornero, A. R. Weily, and Y. J. Guo, "Electronically steerable 1-D Fabry–Pérot leaky-wave antenna employing a tunable high impedance surface," *IEEE Trans. Antennas Propag.*, vol. 60, no. 11, pp. 5046–5055, Nov. 2012.
[19] I. Russo, D. Gaetano, L. Boccia, G. Amendola, and G. Di Massa, "Investigation on the transmission beam-steering capabilities of tunable impedance surfaces," in *Proc. Eur. Microw. Conf. (EuMC)*, Rome, Italy, 2009, pp. 1033–1036.
[20] F. Costa, A. Monorchio, S. Talarico, and F. M. Valeri, "An active high-impedance surface for low-profile tunable and steerable antennas," *IEEE Antennas Wireless Propag. Lett.*, vol. 7, pp. 676–680, 2008.
[21] M. Mavridou, K. Konstantinidis, and A. P. Feresidis, "Continuously tunable mm-wave high impedance surface," *IEEE Antennas Wireless Propag. Lett.*, vol. 15, pp. 1390–1393, 2016.
[22] M. Sazegar *et al.*, "Beam steering transmitarray using tunable frequency selective surface with integrated ferroelectric varactors," *IEEE Trans. Antennas Propag.*, vol. 60, no. 12, pp. 5690–5699, Dec. 2012.
[23] M. I. Abbasi, M. H. Dahri, M. H. Jamaluddin, N. Seman, M. R. Kamarudin, and N. H. Sulaiman, "Millimeter wave beam steering reflectarray antenna based on mechanical rotation of array," *IEEE Access*, vol. 7, pp. 145685–145691, 2019.
[24] M. Mavridou, A. P. Feresidis, P. Gardner, and P. S. Hall, "Tunable millimetre-wave phase shifting surfaces using piezoelectric actuators," *IET Microw., Antennas Propag.*, vol. 8, no. 11, pp. 829–834, Aug. 2014.
[25] M. Mavridou, "Tunable microwave and millimetre-wave metamaterial structures and applications," Ph.D. dissertation, Dept. Electron. Elect. Syst. Eng., Univ. Birmingham, Birmingham, U.K., 2015.
[26] A. P. Feresidis, M. S. Rabbani, and J. Churm, "Tunable piezo-actuated metasurfaces for millimeter-wave and THz antennas," in *Proc. IEEE Int. Symp. Antennas Propag., USNC/URSI Nat. Radio Sci. Meeting*, Boston, MA, USA, Jul. 2018, pp. 1469–1470.
[27] J. Churm, M. S. Rabbani, and A. Feresidis, "Design of millimetre wave phase shifting periodic metasurfaces," in *Proc. 12th Eur. Conf. Antennas Propag. (EuCAP)*, London, U.K., 2018, pp. 1–4.
[28] M. S. Rabbani, J. Churm, and A. Feresidis, "Metamaterial antennas for 5G and beyond," in *Antennas and Propagation for 5G and Beyond*, vol. 35. London, U.K.: Institution of Engineering and Technology, 2020, pp. 35–65.
[29] K. Konstantinidis, "Multi-layer periodic surfaces and metasurfaces for high-gain antennas," Ph.D. dissertation, Dept. Electron. Elect. Syst. Eng., Univ. Birmingham, Birmingham, U.K., 2015.
[30] R. Bancroft, *Microstrip and Printed Antenna Design*. Raleigh, NC, USA: SciTech Publications, 2009.
[31] M. S. Rabbani and H. Ghafouri-Shiraz, "Dual-layer partially reflective surface antennas based on extended size unit cells for 60 GHz band WLAN/WPAN," *IET Microw., Antennas Propag.*, vol. 12, no. 5, pp. 789–795, Apr. 2018.
[32] M. S. Rabbani and H. Ghafouri-Shiraz, "Dual frequency selective surface high gain antenna with deep resonant cavity and E-field reflectors," *Microw. Opt. Technol. Lett.*, vol. 59, no. 11, pp. 2772–2777, Nov. 2017.
[33] K. R. Jha and G. Singh, "Analysis of the effect of ground plane size on the performance of a probe-fed cavity resonator microstrip antenna," *Wireless Pers. Commun.*, vol. 71, no. 2, pp. 1511–1521, Jul. 2013.
[34] D. R. Jackson and A. A. Oliner, "A leaky-wave analysis of the high-gain printed antenna configuration," *IEEE Trans. Antennas Propag.*, vol. 36, no. 7, pp. 905–910, Jul. 1988, doi: 10.1109/8.7194.
[35] A. P. Feresidis, G. Goussetis, S. Wang, and J. C. Vardaxoglou, "Artificial magnetic conductor surfaces and their application to low-profile high-gain planar antennas," *IEEE Trans. Antennas Propag.*, vol. 53, no. 1, pp. 209–215, Jan. 2005, doi: 10.1109/TAP.2004.840528.
[36] G. Goussetis, A. P. Feresidis, and J. C. Vardaxoglou, "Tailoring the AMC and EBG characteristics of periodic metallic arrays printed on grounded dielectric substrate," *IEEE Trans. Antennas Propag.*, vol. 54, no. 1, pp. 82–89, Jan. 2006, doi: 10.1109/TAP.2005.861575.
[37] G. Von Trentini, "Partially reflecting sheet arrays," *IRE Trans. Antennas Propag.*, vol. 4, no. 4, pp. 666–671, Oct. 1956.
[38] P. Kosmas, A. P. Feresidis, and G. Goussetis, "Periodic FDTD analysis of a 2-D leaky-wave planar antenna based on dipole frequency selective surfaces," *IEEE Trans. Antennas Propag.*, vol. 55, no. 7, pp. 2006–2012, Jul. 2007.
[39] J. R. Kelly, T. Kokkinos, and A. P. Feresidis, "Analysis and design of sub-wavelength resonant cavity type 2-D leaky-wave antennas," *IEEE Trans. Antennas Propag.*, vol. 56, no. 9, pp. 2817–2825, Sep. 2008.
[40] A. Mehdipour, J. W. Wong, and G. V. Eleftheriades, "Beam-squinting reduction of leaky-wave antennas using Huygens metasurfaces," *IEEE Trans. Antennas Propag.*, vol. 63, no. 3, pp. 978–992, Mar. 2015.
[41] Y. Ji, L. Ge, J. Wang, Q. Chen, W. Wu, and Y. Li, "Reconfigurable phased-array antenna using continuously tunable substrate integrated waveguide phase shifter," *IEEE Trans. Antennas Propag.*, vol. 67, no. 11, pp. 6894–6908, Nov. 2019.
[42] S. Bildik, S. Dieter, C. Fritzsch, W. Menzel, and R. Jakoby, "Reconfigurable folded reflectarray antenna based upon liquid crystal technology," *IEEE Trans. Antennas Propag.*, vol. 63, no. 1, pp. 122–132, Jan. 2015.

**Muhammad Saqib Rabbani** received the M.Sc. degree in communications engineering and networks and the Ph.D. degree in wireless communications and sensors from the University of Birmingham, Birmingham, U.K., in 2012 and 2018, respectively.

He has developed compact antennas and filters for emerging short-range broadband mobile communications in dynamic environment, and beam-steering Doppler radar-based remote health monitoring sensors operating at microwave, millimeter-wave, and low-terahertz frequency bands. He is currently a Research Fellow with the Department of Electronic, Electrical and System Engineering, University of Birmingham, working on tuneable metamaterial based reconfigurable antennas for future mobile broadband networks, wireless health monitoring sensors, Internet of Things (IoT) and space applications, at millimeter-wave and terahertz frequencies. He has authored or coauthored more than 40 research articles on antenna design and measurements for wireless technologies.

Dr. Rabbani is a Peer Reviewer of several journals including the IEEE TRANSACTIONS ON ANTENNAS AND PROPAGATION, the IEEE ANTENNAS AND WIRELESS PROPAGATION LETTERS, the IEEE JOURNAL OF BIOMEDICAL AND HEALTH INFORMATICS, the IEEE MICROWAVE AND WIRELESS COMPONENTS LETTERS, *International Journal of E-Collaboration (IJEC)* (Elsevier), and *Electronics and MDPI Sensors* (MDPI).

**James Churm** (Member, IEEE) received the Ph.D. degree in microengineering from the University of Birmingham, Birmingham, U.K., in 2017.

He is part of the Metamaterials Engineering Laboratory, University of Birmingham, with expertise in microfabrication and metamaterials. He specializes in millimeter-wave and terahertz (THz) metamaterial components, focusing on low-loss tuning technologies and fabrication methods. His current research interests center on sub-THz tunable systems for communications and sensing.

**Alexandros P. Feresidis** (Senior Member, IEEE) was born in Thessaloniki, Greece, in 1975. He received the Physics degree from the Aristotle University of Thessaloniki, Thessaloniki, Greece, in 1997, the M.Sc. (Eng.) degree in radio communications and high frequency engineering from the University of Leeds, Leeds, U.K., in 1998, and the Ph.D. degree in electronic and electrical engineering from Loughborough University, Loughborough, U.K., in 2002.

During the first half of 2002, he was a Research Associate and in the same year he was appointed as a Lecturer in wireless communications with the Department of Electronic and Electrical Engineering, Loughborough University, where, in 2006, he was promoted to a Senior Lecturer. In December 2011, he joined the Department of Electronic, Electrical and Systems Engineering, University of Birmingham, Birmingham, U.K., where he is currently a Professor of microwave and terahertz communications. He has authored or coauthored more than 170 articles in peer reviewed international journals and conference proceedings and has coauthored five book chapters. His research interests include analysis and design of metamaterials, electromagnetic bandgap (EBG) structures and frequency selective surfaces (FSS), leaky-wave antennas, small/compact antennas, passive microwave/millimeter-wave/terahertz circuits, microfabrication, and numerical techniques for electromagnetics and bioelectromagnetics.

Dr. Feresidis is a member of the U.K. EPSRC Peer Review College. He has held a Senior Research Fellowship Award from the U.K. Royal Academy of Engineering and The Leverhulme Trust (2013–2014). He was on the Editorial Board of *IET Microwaves, Antennas and Propagation Journal* (2014–2018). He is currently an Associate Editor of the IEEE TRANSACTIONS ON ANTENNAS AND PROPAGATION.